Published in final edited form as:
Mol Microbiol. 2014 August ; 93(3): 453–463. doi:10.1111/mmi.12669.

Differential affinities of MinD and MinE to anionic phospholipid influence Min Patterning dynamics *in vitro*

Anthony G. Vecchiarelli[1], **Min Li**[1], **Michiyo Mizuuchi**[1], and **Kiyoshi Mizuuchi**[1,*]

[1] Laboratory of Molecular Biology, National Institute of Diabetes, and Digestive and Kidney Diseases, National Institutes of Health, Bethesda, MD 20892, USA

Abstract

The *E. coli* Min system forms a cell-pole-to-cell-pole oscillator that positions the divisome at mid-cell. The MinD ATPase binds the membrane and recruits the cell division inhibitor MinC. MinE interacts with and releases MinD (and MinC) from the membrane. The chase of MinD by MinE creates the *in vivo* oscillator that maintains a low level of the division inhibitor at mid-cell. *In vitro* reconstitution and visualization of Min proteins on a supported lipid bilayer has provided significant advances in understanding Min patterns *in vivo*. Here we studied the effects of flow, lipid composition, and salt concentration on Min patterning. Flow and no-flow conditions both supported Min protein patterns with somewhat different characteristics. Without flow, MinD and MinE formed spiraling waves. MinD and, to a greater extent MinE, have stronger affinities for anionic phospholipid. MinD-independent binding of MinE to anionic lipid resulted in slower and narrower waves. MinE binding to the bilayer was also more susceptible to changes in ionic strength than MinD. We find that modulating protein diffusion with flow, or membrane binding affinities with changes in lipid composition or salt concentration, can differentially affect the retention time of MinD and MinE, leading to spatiotemporal changes in Min patterning.

INTRODUCTION

The Min system of *Escherichia coli* functions as a spatial regulator for the placement of the cell division apparatus at mid-cell by forming a cell-pole to cell-pole oscillator that prevents asymmetric division at the nucleoid-free poles (de Boer *et al.*, 1989; Lutkenhaus, 2007). The *E.coli* nucleoid occlusion (NO) system works in concert to prevent cell division over the nucleoid (Woldringh et al., 1991; Bernhardt and de Boer, 2005). Together, the Min and NO systems allow for precise division at mid-cell and the generation of two nearly identical daughter cells after chromosome replication and segregation (Yu and Margolin, 1999).

Surface-mediated protein gradients are emerging as a versatile way to control subcellular organization in bacteria (Vecchiarelli *et al.*, 2012; Kiekebusch and Thanbichler, 2012). Min is a three component system that self-organizes into a spatial oscillator on the inner membrane of *E.coli* (Lutkenhaus, 2007). The MinD ATPase dimerizes in the presence of ATP and binds membrane via an amphipathic helix at its C-terminus (Hu and Lutkenhaus,

[*]Correspondence to: Kiyoshi Mizuuchi Laboratory of Molecular Biology, National Institute of Diabetes, and Digestive and Kidney Diseases, National Institutes of Health Bethesda, MD 20892-0540, USA kmizu@helix.nih.gov.

2003; Szeto *et al*., 2002; Lackner *et al*., 2003; Zhou and Lutkenhaus, 2003; Wu *et al*., 2011). Membrane-associated MinD then recruits its passenger protein MinC (Hu and Lutkenhaus, 2000), which acts as a potent inhibitor of Z-ring formation - a key prerequisite for assembly of the cell division machinery (Bi and Lutkenhaus, 1991). MinD also recruits its ATPase stimulator MinE to the membrane (Hu *et al*., 2002; Raskin and de Boer, 1999). MinE interaction results in the membrane release of MinD and MinC (Hu and Lutkenhaus, 1999). The perpetual chase and membrane release of MinD by MinE generates the remarkable pole-to-pole system oscillation (Raskin and de Boer, 1999b), and a time-averaged concentration minimum of the Z-ring inhibitor at mid-cell (Fu *et al*., 2001; Hale *et al*., 2001). Despite the apparent simplicity of this minimal system, a full understanding of the interactions between Min proteins and the membrane is only recently emerging.

MinD and MinE are sufficient for generating system oscillations *in vivo* (Hu *et al*., 1999; Raskin and de Boer, 1999). Reconstitution of MinD and MinE patterning *in vitro* on supported lipid bilayers (SLBs) made from *E.coli* lipid extracts have provided significant advances in elucidating the underlying mechanism (Loose *et al*., 2008; Ivanov and Mizuuchi, 2010). Min patterns have been reconstituted under two regimes: (i) Under constant flow, whereby the sample was infused into a lipid-coated flowcell (Ivanov and Mizuuchi, 2010), and (ii) under conditions without flow, where the sample was placed in a lipid-coated well (Loose *et al*., 2008). Constant flow supported multiple modes of pattern formation, whereas the well setup produced stable and spiraling wave trains. Temporary mixing of the solution phase in the well by a micropipette did not affect Min patterning on the bottom of the well (Loose *et al*., 2008). Similarly, dynamic patterns persisted in the flowcell setup for multiple cycles after the sample flow was halted (Ivanov and Mizuuchi, 2010). The studies reported that surface patterning is not limited by Min protein diffusion in the solution phase, which suggests spatial inhomogeneity of Min protein concentration in solution is not a critical determinant for patterning. Therefore under the small confines of a bacterial cell, where proteins diffuse rapidly in the cytoplasm (Mika and Poolman, 2011), the relatively slower Min patterning dynamics on the membrane can persist even when the Min protein distribution in the cytoplasm is spatially homogenous. Here we extended our flowcell-based study, focusing on the wave mode of Min patterning observed on the SLB, to examine the impact of changes in the solution phase in more detail. We find that altering the solution diffusion/dispersion conditions of MinD and MinE can dramatically affect Min wave organization on the SLB. Our analysis here both explains and unifies the modes of patterning observed previously in both regimes, thus enabling us to further study the mechanistic details that govern Min patterning *in vivo*.

Like MinD, MinE also has a membrane-targeting sequence (MTS) essential for the spatial regulation of cell division *in vivo* (Hsieh *et al*., 2010). It is still uncertain how membrane-binding by MinE contributes to the patterning mechanism because of the difficulty in differentiating the membrane binding activities of both MinD and MinE in bulk biochemical assays (Renner and Weibel, 2012). Structural studies suggest MinE binding to membrane-bound MinD unveils its cryptic N-terminal MTS (Park *et al*., 2011). However, MinE can also bind directly to anionic phospholipid without MinD *in vitro* (Hsieh *et al*., 2010; Renner and Weibel, 2012), and single molecule studies have shown MinE can remain bound after

MinD has detached from an SLB (Loose et al., 2011). A number of models for Min patterning have suggested lipid composition may affect how the Min proteins act as spatial regulators (Cytrynbaum and Marshall, 2007; Drew *et al*., 2005). Here we directly visualize how lipid composition and ionic interaction between the lipid bilayer and Min proteins influence their patterning dynamics on the SLB.

RESULTS

Flow influences Min patterning on an SLB

When 1 μM GFP-MinD and 1.5 μM MinE (mixed 1:19 with MinE-Alexa 647) were preincubated with ATP and infused into a flowcell coated with *E.coli* lipid, patterns initiated with GFP-MinD cooperatively binding the membrane as radially expanding and circular initiation centers (Fig. 1A). MinE binding followed at the initial site of MinD binding, that is, in the center of the radially expanding circle. With continual flow (1 μl/min, 25 μm × 4 mm cross section), radial expansion became asymmetric, creating a MinD wave that propagated upstream and was chased by an increasing concentration of MinE (Fig. 1A, Movie S1). At the tail end of the wave, both protein concentrations fell off sharply followed by a valley of low protein binding. Several waves continued to propagate upstream until downstream waves caught up to the tail end of upstream waves (Fig. S1, Movie S2). At this point, the pattern switched to a surface concentration oscillation of bilayer-bound MinD and MinE over a broad area of the SLB. This oscillation-mode persisted while flow was maintained. These modes of Min patterning under constant flow have been thoroughly characterized in our previous *in vitro* reconstitution study (Ivanov and Mizuuchi, 2010).

Why do Min waves travel in the opposite direction of flow? As MinD initiation zones expanded, the center of the zone accumulated enough MinE to trigger MinD/E dissociation from the bilayer. One might have expected a fully circular wave to develop. Instead, with flow, the downstream-facing half of the expanding MinD circle disappeared. This, we believe, is due to dissociating MinE molecules from the center of the zone rapidly rebinding the SLB immediately downstream. These MinE molecules may have their MTS- and MinD-interaction interfaces exposed, and are therefore still active for MinD removal from the SLB. While the downstream-facing half of the MinD circular zone is removed from the SLB, the upstream-facing half is left unhindered to expand into a propagating wave that travels upstream. Upstream-propagating waves organize into wave trains (Movie S2). Therefore this downstream-acting MinE must be short lived because the following waves are not wiped out by the “active” MinE molecules released from the tail of the leading wave. The short lifetime of this active MinE may reflect the transition time required for MinE to revert to its closed conformation, where the MTS- and MinD-interaction interfaces become masked (Park *et al.*, 2011).

Upon flow stoppage, the oscillations turned into highly regular spirals over the course of several minutes (Fig. 1B, Movie S3). The patterning was very similar to that which has been reported previously in the absence of flow (Loose *et al.*, 2008). The outward propagating wave trains of a spiral were composed of spatially periodic and staggered peaks of membrane-bound MinD and MinE separated by valleys of low protein concentration (Fig. 1C), which persisted many hours after flow stoppage with an ATP regeneration system (Fig.

1D and data not shown). The surface concentration distribution of membrane-bound MinD and MinE within a cross section of the wave trains, or within a time trajectory through wave cycles, are all qualitatively similar to the previous reports (Ivanov and Mizuuchi, 2010; Loose *et al.*, 2011). Together, the results show that changes in the diffusion/dispersion of reaction components in solution can dramatically affect the Min wave organization on SLBs and explains the differences in Min patterning observed previously under flow and no-flow conditions.

Cardiolipin is not necessary for Min patterns

The *E.coli* polar lipid extract used for SLB formation is composed of 67% phosphatidylethanolamine (PE), 23.2% phosphatidylglycerol (PG), and 9.8% Cardiolipin (CL) (weight %; Avanti Polar Lipids). We set out to determine the effects of lipid composition on Min patterning on SLBs. We first made a synthetic bilayer composed of a minimal number of lipid types that still supported the Min patterns observed on *E. coli* lipid. PE is the main zwitterionic lipid found in *E.coli*. We replaced PE with phosphatidylcholine (PC) as the net-charge neutral lipid in the bilayer because PC showed less aggregation in solution, a more uniform SLB, and greater membrane fluidity at the room temperature for our experiments (~24°C). PG is an anionic lipid with a net charge of -1. CL is also anionic with the potential of carrying two negative charges. However, under physiological conditions CL has been proposed to have a charge of -1 (Lewis and McElhaney, 2009). We replaced CL with more PG to roughly maintain the same negative charge density as that of the *E.coli* lipid bilayer. Therefore our minimal supported lipid bilayer (mSLB) was composed of 67% PC and 33% PG (mol %).

Min patterns on the mSLB were essentially identical to that found on *E.coli* lipid (Fig. 2). With flow, MinD initiation centers asymmetrically broke into waves that propagated upstream with an increasing surface concentration of MinE toward the trailing edge of the waves (Fig. 2A, Movie S4). The waves then transitioned into oscillation-mode. Upon flow stoppage, the mSLB supported spirals (Fig. 2B, C; Movie S5) that persisted for many hours (Fig. 2D and data not shown). It has been previously shown that the MinD waves within a spiral are thinner and propagate faster with increasing MinE concentration (Loose *et al.*, 2008). Under no-flow conditions in our flowcell setup, we find the same MinE concentration dependence on both *E. coli* lipid and the mSLB (Fig. 2E, F and Fig. S2). The findings show that CL is not specifically required for Min patterning initiation or maintenance on a planar lipid bilayer.

Anionic lipid density of the SLB influences Min patterns

The finding that CL was not specifically required for Min patterning *in vitro* implied that it is the anionic charge density of the bilayer, and not a specific lipid type, that influences Min patterning. We made bilayers with varying densities of negative charge by using PC as the zwitterionic lipid and titrated PG to test the effects of anionic lipid density on Min patterns. Min protein wave patterning was robust over a wide range of PG concentrations, from 0 % (DOPC alone) to 63% PG (Fig. 3A). The amount of both MinD and MinE making up the patterns on the bilayer correlated with increasing PG, showing that anionic lipid increases membrane binding of both proteins (Fig. 3B). Consistent with this finding, MinE-stimulated

MinD ATPase activity in the presence of liposomes was lower with low PG content (≤ 13 % PG) when compared to liposomes with ≥ 23% PG (Fig. S3A). With increasing PG, MinD bands became narrower and slowed in velocity (Fig. 3C). At 63% PG, MinD bands still formed but were short lived, and did not propagate into stable spirals (Fig. 3A). At 73% PG, no patterns were observed. The staggered protein concentration peaks of MinD and MinE at the rear of a wave displayed a MinD:MinE molar ratio of approximately 1:1 at all PG densities that supported wave formation (Fig. 3D). However with increasing PG, a higher concentration of MinE remained in the troughs between waves after dissociation of MinD from membrane (Fig. 3E). The data suggest that high PG concentrations promote membrane binding by MinE, which shortens the MinD wavelength, decreases wave velocity, and is responsible for halting Min patterns at very high PG densities. We conclude that Min patterning is robust over a wide range of anionic lipid densities, which is consistent with the ability of the Min system to form patterns in heterologous bacteria with significantly different anionic lipid compositions (Ramirez-Arcos *et al*., 2002; Jamroskovic *et al*., 2012). The results are also consistent with the idea that Min proteins may preferentially dwell at the poles of the *E.coli* cell where anionic lipid content has been shown to be higher (Dowhan *et al*., 2004; Dowhan and Mileykovskaya, 2005; Renner and Weibel 2012).

We went one step further and created a synthetic bilayer with lipids predominantly found in eukaryotic membranes, and not present in *E.coli*. We continued to use 67% PC as the net-charge neutral lipid, and replaced PG with 33% phosphatidylserine (PS) as the anionic phospholipid. The PC/PS bilayer supported wave trains similar to that formed on the mSLB as well as on the *E.coli* lipid bilayer (Fig. 3F, Movie S6). The data further shows that it is the charge density and not the specific lipid head group that influences Min patterning.

Salt Effects on Min Patterns

Changing the lipid composition of the SLB can not only affect electrostatic interactions, but also the mechanical properties of the membrane. By titrating the salt concentration while keeping the anionic lipid composition of the bilayer constant, we further tested how changes in electrostatic interactions between Min proteins and the bilayer can alter patterning. Taking into account salt addition from protein stocks, our typical experiments are performed at 170 mM KCl. Under these standard conditions (1 μM MinD and 1.5 μM MinE), MinD wave bands are ~20 μm wide and travel at a velocity of ~10 μm/min on the mSLB or the *E.coli* bilayer (see Fig. 2E, F). Varying the salt concentration from 50 to 500 mM KCl had dramatic effects on Min patterning (Fig. 4A-B). Increasing salt showed the same effect as decreasing the PG content of the lipid bilayer – MinD wave bands became wider and wave velocity faster (Fig. 4C). Decreasing the salt concentration showed the same effect as increasing PG - MinD bands became narrower and slowed in velocity. The staggered protein concentration peaks of MinD and MinE at the rear of a wave displayed a MinD:MinE molar ratio of roughly 1:1 at 100 mM KCl, but MinE concentration fell more precipitously than MinD at higher salt concentrations (Fig. 4D). In the troughs between waves, MinE association with the lipid bilayer was significantly stronger than MinD at lower salt (Fig. 4E). Together with the PG titration results, the data further shows that both Min proteins associate with the lipid bilayer in part via electrostatic interaction. However, MinE binding is more selective towards anionic lipid, which allows for stable membrane binding of MinE

independent of MinD at low ionic strength. The findings support a mechanism whereby MinE has the ability to "linger" on the membrane after MinD is released. The remaining MinE perhaps acts as a dissociation complex that prevents MinD rebinding at the old pole, thus indirectly promoting *de novo* MinD binding to the opposing pole.

MinD ATPase activity, with or without MinE, did not significantly change with varying salt concentration (Fig. S3B). The data show ATP-hydrolysis by MinD and stimulation by MinE are not significantly affected, and are therefore not directly responsible for Min pattern variation within the range of salt concentrations tested here.

DISCUSSION

We have shown here and in a previous report (Ivanov and Mizuuchi, 2010) that MinD and MinE can form a variety patterns under constant flow. Here we further studied changes in the wave-type patterns after flow was stopped. When the reaction mix was infused into a fresh lipid-coated flow cell at 1 μl/min, MinD bound as radially expanding circular zones, followed by MinE accumulation starting from the center of the circular zone. The circular zone underwent a symmetry breaking event and transitioned into a propagating wave that traveled upstream as an increasing concentration of MinE both chased and removed MinD at the tail end of the wave. Over time, multiple waves coalesce to form a locally synchronized oscillation of MinD binding, followed by MinE accumulation, and then the dissociation of both proteins. Stopping the sample flow induced a pattern transition to regular and stable wave spirals reported previously as the most typical dynamic pattern observed in the absence of flow (Loose *et al*., 2008).

In our previous study of Min patterning in the presence of flow (Ivanov and Mizuuchi, 2010), the origin of wave initiation was not studied in detail. Under the previous experimental conditions, surface patterning in many experiments started with a near simultaneous initiation and fusion of multiple MinD binding centers within close proximity. The coalescence of initiation centers led to a rapid transition to the "oscillation" mode of patterning, thus precluding observations of the symmetry breaking event we report here. Other than this minor difference, the two studies are in general agreement regarding Min pattern formation in the presence of flow.

Isolated MinD initiation centers expanded as the center of the zone accumulated a sufficient MinE concentration to trigger MinD/E dissociation from the bilayer. In the presence of flow, the downstream-facing half of the expanding circle disappeared. We believe this indicates the presence of a diffusible active state of MinE that is short-lived and catalyzes the dissociation of MinD in the downstream-facing half of the circular zone. MinE has been shown to undergo dramatic structural transitions to unveil its MinD- and membrane-interaction interfaces (Park *et al*., 2011). We believe this "active" form of MinE is the diffusible MinD-dissociation catalyst. The transiency of this active state may correspond with the time needed for MinE to revert back to its latent form. The upstream-facing half of the circle is left unhindered to expand into a propagating wave with its direction of travel roughly confined to within the upstream half of the arc. The results provide an explanation for the differences in wave patterning observed previously under flow- (Ivanov and

Mizuuchi, 2010) and no-flow conditions (Loose *et al*., 2008). Other than the wave orientation bias, the general properties of Min waves were not noticeably influenced by flow.

Min waves were strongly influenced by the lipid composition of the SLB. The differences in patterns with varying SLB compositions unveiled several fundamental properties of MinD and MinE membrane binding activity, and showed how these activities contribute to the *in vivo* patterning mechanism in different ways. Both MinD, and to a greater extent MinE, clearly have stronger affinities for anionic phospholipids. Our experiments are consistent with previous studies that measured MinD and MinE protein binding to liposomes and SLBs of varying lipid composition (Hsieh *et al*., 2010; Mileykovskaya *et al*., 2003; Renner and Weibel, 2012). Here we extended these biochemical studies by directly visualizing how lipid composition and salt concentration can impact the self-organized Min patterns on an SLB. Min wave patterning was robust over a wide range of anionic lipid densities (0 to 53 % PG) and salt concentrations (100 to 500 mM KCl). Increasing anionic lipid or decreasing salt resulted in shorter wavelengths and a slower wave velocity. Surface protein density analysis found that both MinD and MinE concentrations within a wave concomitantly increased with increasing negative charge density on the SLB or, to a lesser degree, with decreasing salt concentration in solution. However in the troughs between waves, the surface-bound MinE concentration became significantly higher than that of MinD. With a highly negatively charged bilayer (> 53% PG) or with very low salt (50 mM KCl), MinE bound the bilayer independent of MinD and Min waves did not persist. Considering the mirroring influence of lower ionic strength of the reaction buffer and higher negative charge density of the bilayer, we conclude the narrower and slower Min waves at high PG densities are due to increased bilayer binding of MinE that triggers MinD dissociation. MinD-independent MinE binding to the bilayer slows the wave velocity and narrows the wavelength, and at very high PG concentrations in the bilayer, or at low ionic strengths in solution, the background MinE binding halts patterning altogether. *In vivo*, a low level of membrane-bound MinE that "lingers" at the cell pole after MinD has been removed may prevent MinD from re-initiating the new membrane binding cycle at the pole from which it just dissociated, thus promoting *de novo* MinD binding to the opposing pole.

CL is an anionic phospholipid widely found in bacterial membranes and in mitochondria, which preferentially distributes to areas of negative membrane curvature (Renner and Weibel, 2011), such as the poles and septa of rod-shaped bacteria (Bernal *et al*., 2007; Kawai *et al*., 2007; Mileykovskaya and Dowhan, 2000). It has been proposed that polarly localized CL may act as a spatial cue for pole-to-pole Min patterning *in vivo* (Dowhan and Mileykovskaya, 2005; Renner and Weibel, 2011). Stronger associations with anionic phospholipids, enriched at the poles (Koppelman *et al*., 2001), may play a role in prolonging MinD and MinE at the pole prior to MinE-stimulated release and relocation of MinD to the opposing pole (Mileykovskaya and Dowhan, 2000; Mileykovskaya *et al*., 2003; Renner and Weibel, 2012). However, in filamentous cells the Min system forms a standing-wave zebra pattern, suggesting such polar determinants are not critical (Raskin and de Boer, 1999). Also, at comparable concentrations of anionic phospholipids, no preference for MinD binding to CL versus PG was found (Renner and Weibel, 2012). We find here that CL and

its possible steric effects, which have been proposed to correlate membrane curvature with MinD localization (Renner and Weibel , 2011), are not specifically necessary for initiating or maintaining Min patterns *in vitro*. Rather it is the negative charge density of the SLB that strongly influences the system dynamics. Furthering this point, we found Min patterns were supported on bilayers made with PC and PS; phospholipids prevalent in eukaryotic membranes, but not in *E.coli*. The *in vitro* data are consistent with a *pgsA* null mutant of *E. coli*, which lacks PG and CL and are partially substituted by their precursor anionic lipids, yet displays unaltered Min oscillations *in vivo* (Mileykovskaya *et al*., 2009).

Heterologous expression of *E.coli* MinD and MinE proteins in *Bacillus subtilis* supported system oscillations that had a periodicity 1.5-3.5 times slower than that found in *E.coli* (Jamroskovic *et al*., 2012). The decrease did not seem to be due to differences in protein expression or off-target effects with host proteins. Intriguingly, the phospholipid composition of *B. subtilis* is significantly higher in both CL and PG compared to that of *E. coli* (Lopez *et al*., 2006). In *E.coli* cells lacking PE, the high density of anionic lipid resulted in the formation of MinD foci, as opposed to polar zones, that disappear in concert with the appearance of a new MinD focus in close proximity (0.5 to 1 μm) - considerably shorter spatial parameters than the dynamic Min patterns observed in cells with normal lipid composition (Mileykovskaya *et al*., 2003). Our results here suggest that the greater density of anionic lipid could explain the slower rate of wave propagation, and the slower oscillatory period of Min proteins observed *in vivo*.

Both MinD and MinE bind the membrane via amphipathic helices that are critical to Min oscillation and divisome positioning *in vivo* (Hu and Lutkenhaus, 2003; Szeto *et al*., 2003). Electrostatic interactions are one of several forces taking part in the membrane association. The prevailing notion is that the helices become ordered upon interaction with the membrane and membrane adsorption is facilitated by non-specific charge interaction and diffusion (Cho and Stahelin, 2005). This is subsequently stabilized through membrane penetration and hydrophobic interaction. It has been proposed that MinD binding to ATP and dimerization is required for its membrane binding activity via a C-terminal MTS (Szeto *et al*., 2002; Szeto *et al*., 2003), and MinE binding to membrane-bound MinD unveils the cryptic N-terminal MTS of MinE (Park *et al*., 2011). MinE, however, can also bind anionic phospholipid directly without MinD *in vitro* (Hsieh *et al*., 2010; Renner and Weibel, 2012). We find that MinD binding and, to a greater extent, MinE binding to the SLB is enhanced by ionic interaction. But, at high PG density or low salt concentration, MinE strongly binds the SLB independent of MinD. This activity significantly shortens the wavelength and slows the wave velocity.

The MTS of MinD is an amphipathic helix that provides both positively charged residues for electrostatic interaction with the head groups of anionic phospholipids as well as a hydrophobic face for interaction with the membrane (Zhou and Lutkenhaus, 2003). The MTS of MinE consists of an amphipathic helix and an adjacent patch of positively charged residues (Hsieh *et al*., 2010; Shih *et al*., 2011). MinE binding was significantly more susceptible to changes in ionic strength than MinD, suggesting that charge interactions play a greater role in membrane binding by MinE. Our data is consistent with previous results showing that membrane binding by the MTS of MinD is resistant to high ionic strength *in*

vitro (Hu and Lutkenhaus, 2003). We conclude the differing mechanisms of membrane binding by the MTSs of MinD and MinE differentially affect the retention time of the two proteins, thus leading to both spatial and temporal changes in Min patterning on membranes of varying lipid composition.

EXPERIMENTAL PROCEDURES

Proteins

Protein expression, purification, and labeling were performed essentially as described previously (Ivanov and Mizuuchi, 2010). The genes *his6-egfp-minD* and *his6-minD* were cloned into pET100/D-TOPO to create the expression plasmids pOld and pXO5, respectively (Ivanov and Mizuuchi, 2010). *minE-his* was cloned into the expression vector pET41a (pXO9). Plasmids were transformed into BL21 (AI) cells (Invitrogen) for protein expression. Overnight cultures were used to inoculate LB broth with 100 μg/ml carbinecillin, which then was incubated with aeration at 20°C to an OD_{600} of ~0.6. Protein expression was induced with 1 mM isopropylthio-β-galactoside and 0.2 % arabinose, and the cells were grown at 16°C overnight. The cells were pelleted, frozen with liquid nitrogen, and stored at −80°C. Cell pellets were resuspended in lysis buffer and lysed using a microfluidizer. Lysates were cleared by centrifugation and filtration, loaded onto a 5 mL HiTRAP HP Ni column (GE Healthcare), and protein was eluted by an imidazole gradient. For all proteins, the peak fractions were pooled, concentrated, and passed over a Superdex200 (His6-MinD and His6-eGFP-MinD) or Superdex75 (MinE-His6) column equilibrated with storage buffer (MinE storage buffer - 25 mM Hepes-KOH pH 7.6, 0.3 M KCl, 0.1 mM EDTA, 10% vol/vol Glycerol, 2 mM DTT; MinD protein storage buffer - 50 mM Hepes-KOH pH 7.6, 0.5 M KCl, 0.1 mM EDTA, 10% vol/vol Glycerol, 2 mM DTT). Proteins were concentrated, frozen with liquid nitrogen, and stored at −80 °C.

MinE-His6 was dye coupled by first adding 10 mM DTT to the unlabeled protein stock, followed by exposure to nitrogen gas. DTT was then removed from the sample using a Superdex75 column equilibrated in MinE storage buffer without DTT. MinE-His6 was then incubated with Alexa Fluor 647 dye C_2-maleimide (Invitrogen) at a 2:1 dye:protein molar ratio for 30 min at 23°C. The labeling reaction was quenched with 10 mM DTT, and free label was removed using a Superdex75 column equilibrated with MinE storage buffer. The labeled protein was concentrated and average labeling efficiency was determined with a NanoDrop spectrophotometer by comparing absorbencies at 280 nm and 647 nm. The average labeling efficiency was calculated to be ~ 60%.

Flowcell Assembly

Flowcells were assembled as described previously (Vecchiarelli *et al.*, 2013). Fused silica slides with drilled inlet and outlet holes (Esco Products) were washed with NOCHROMIX glass cleaner (Sigma), rinsed with deionized water, air dried, and treated with low-power plasma cleaning in the presence of argon and oxygen. A 4 mm-wide by 3 cm-long flow channel was cut on a piece of 25 μm-thick acrylic transfer tape (3M), which was placed between a glass cover slip and the slide. Nanoports (Upchurch) were attached to the slides above the holes with optical adhesive. The flowcell was then baked at 100°C for 45 min.

Supported Lipid Bilayer

E. coli Polar Lipid Extract (Cat. #100600) and monounsaturated (18:1) synthetic lipids 1,2-dioleoyl-*sn*-glycero-3-phosphocholine (DOPC; Cat. # 850375), 1,2-dioleoyl-*sn*-glycero-3-[phospho-*rac*-(1-glycerol)] (DOPG; Cat. # 840475), and 1,2-dioleoyl-*sn*-glycero-3-phospho-L-serine (DOPS; Cat. # 840035) were purchased from Avanti dissolved in chloroform at 25 mg/ml. The synthetic lipids were mixed in glass tubes pre-rinsed with chloroform to the compositions indicated. Chloroform was evaporated under dry N_2 gas with tube rotation. The lipid film was dried further in a SpeedVac Concentrator (Savant) for 2.5 hours. Under N_2 atmosphere, the lipid film was resuspended in degassed TK150 buffer (25 mM Tris-HCl, pH 7.4, 150 mM KCl) to a lipid concentration of 5 mg/ml. The tube top was wrapped in parafilm for overnight lipid hydration at 23°C. The lipids were then vortexed for 1 minute, and sonicated at 23°C in a water bath sonicator at 70W for 15 minutes (2 min/pulse with 30 sec rest) or until blue-shifted translucence is apparent (~100 nm Small Unilamellar Vesicles, SUVs). Under N_2 atmosphere, the SUVs were passed through a 0.2 micron filter and aliquoted into Teflon-capped and parafilm-sealed vials for storage at 4°C. SUV stocks were typically used within two weeks from the preparation date.

To make the SLB, 100 μl SUV stock was diluted to 1 mg/ml with 400 μl TK150 buffer. Five millimolar $MgCl_2$ was added to the sample, which was then transferred to a syringe. Roughly 400 μl of the diluted sample was slowly infused into a flowcell pre-warmed to 37°C. The flowcell was maintained at 37°C in a temperature controlled chamber. After 1 hour incubation, 400 μl of pre-warmed TK150 buffer + 5 mM $MgCl_2$ was infused at a rate of 100 μl/min to wash the SLB. The lipid-coated flowcells were kept at 37°C until mounted on the microscope stage.

Sample handling and preparation

Experiments were performed in Min buffer: 25 mM Tris-HCl, pH 7.4, 150 mM KCl, 5 mM $MgCl_2$, 2 mM DTT, and 0.5 mg/ml ascorbic acid. Five millimolar phosphoenolpyruvate (Sigma) and 10 μg/mL pyruvate kinase (Sigma) were also added for ATP regeneration. The salt titration experiments were also performed in Min buffer, but with varying KCl concentrations as specified.

At the concentrations indicated, GFP-MinD was preincubated with MinE (mixed 1:19 with MinE-Alexa 647) in Min buffer for 15 minutes at 23°C before the addition of 2.5 mM ATP. The 500 μl sample was then passed through a 0.2 micron amicon filter, and loaded into a 1 ml syringe. TFZL 1/16” × 0.02” tubing (UpChurch) was used to connect the syringe to the flow cell inlet nanoport (UpChurch). Samples were infused into the flowcell using a neMESYS syringe pump (Cetoni) at 1 μl/min, which equates to a cross-sectional velocity of ~ 0.17 mm/sec.

Imaging and Analysis

Illumination, microscope, and camera settings were described previously (Ivanov and Mizuuchi, 2010). A prism-type TIRFM setup was used with an Eclipse TE2000E microscope (Nikon) with a PlanApo 10× (NA = 0.45, air) or 40× (NA = 1.0, oil-immersed) objective. Andor DU-897E camera settings were digitizer, 3 MHz (14-bit gray scale);

preamplifier gain, 5.2; vertical shift speed, 2 MHz; vertical clock range: normal, electron-multiplying gain 40, EM CCD temperature set at −98 °C, baseline clamp ON, exposure time 100 ms. The setup for single-molecule acquisition (see Protein Density Estimation) was similar except that the electron-multiplying gain was 200, vertical shift speed was 1.11 MHz, and frame rate was 10 Hz. All movies were acquired through a DualView (Photometrics) with dcxr630 insert for two-color acquisition. The baseline of ~100 camera units was subtracted from the data.

The excitation for GFP-MinD and MinE-Alexa647 was provided by a 488 nm diode-pumped solid-state laser (Sapphire, Coherent) at 8 μW and a 633 nm HeNe laser (Research Electro-Optics) at 300 μW, respectively. TIRF illumination had a Gaussian shape in the field of view, therefore intensity data for bilayer-bound populations of GFP-MinD and MinE-Alexa647 were taken at or near the middle of the illumination profile.

Movies were acquired using Metamorph 7 (Molecular Devices) and transferred to ImageJ (National Institutes of Health) for analysis and conversion to QuickTime file format (.mov). Brightness and contrast were set for each picture or movie individually for the best representation of the features of interest. However, panels within a single movie share the same settings. All movies were acquired at 5 seconds/frame and accelerations are indicated in the movie legends. Adobe illustrator was used to convert movies into figures.

Protein Density Estimation

GFP-MinD (50 pM) was incubated with 0.5 μM MinD and 1 mM ATP in Min Buffer at 23°C for 15 min. The sample was then infused into the mSLB-coated flowcell, and single GFP-MinD molecules were illuminated on the bilayer surface using a 488 nm laser at 7.1 mW. MinE-Alexa647 (50 pM) was mixed with 0.5 μM MinE in Min Buffer and infused into a flowcell coated with a bilayer composed of 63% PG + 37% PC to promote MinD-independent MinE binding to the bilayer surface. Single MinE-Alexa647 molecules were illuminated using a 633 nm laser at 9 mW. The average fluorescence intensity of single GFP-MinD or MinE-Alexa647 molecules were measured and used to calculate the number of fluorescent dimers within a region of interest to obtain a protein density expressed as dimers/μm^2.

Supplementary Material

Refer to Web version on PubMed Central for supplementary material.

Acknowledgments

This work was supported by the intramural research fund for National Institute of Diabetes and Digestive and Kidney Diseases (to K.M.) and the Nancy Nossal Fellowship (to A.G.V.).

REFERENCES

Bernal P, Muñoz-Rojas J, Hurtado A, Ramos JL, Segura A. A *Pseudomonas putida* cardiolipin synthesis mutant exhibits increased sensitivity to drugs related to transport functionality. Environ Microbiol. 2007; 9:1135–1145. [PubMed: 17472630]

Bernhardt TG, de Boer PAJ. SlmA, a Nucleoid-Associated, FtsZ Binding Protein Required for Blocking Septal Ring Assembly over Chromosomes in *E. coli*. Mol Cell. 2005; 18:555–564. [PubMed: 15916962]

Bi E, Lutkenhaus J. FtsZ ring structure associated with division in *Escherichia coli*. Nature. 1991; 354:161–164. [PubMed: 1944597]

Cho W, Stahelin RV. Membrane-protein interactions in cell signaling and membrane trafficking. Annu Rev Biophys Biomol Struct. 2005; 34:119–151. [PubMed: 15869386]

Cytrynbaum EN, Marshall BDL. A Multistranded Polymer Model Explains MinDE Dynamics in *E. coli*. Cell Division. Biophys J. 2007; 93:1134–1150.

de Boer PAJ, Crossley RE, Rothfield LI. A division inhibitor and a topological specificity factor coded for by the minicell locus determine proper placement of the division septum in *E. coli*. Cell. 1989; 56:641–649. [PubMed: 2645057]

Dowhan W, Mileykovskaya E, Bogdanov M. Diversity and versatility of lipid–protein interactions revealed by molecular genetic approaches. Biochim Biophys Acta. 2004; 1666:19–39. [PubMed: 15519306]

Dowhan W, Mileykovskaya E. Role of membrane lipids in bacterial division-site selection. Curr Opin Microbiol. 2005; 8:135–142. [PubMed: 15802243]

Drew DA, Osborn MJ, Rothfield LI. A polymerization-depolymerization model that accurately generates the self-sustained oscillatory system involved in bacterial division site placement. Proc Natl Acad Sci USA. 2005; 102:6114–6118. [PubMed: 15840714]

Fu X, Shih Y-L, Zhang Y, Rothfield LI. The MinE ring required for proper placement of the division site is a mobile structure that changes its cellular location during the *Escherichia coli* division cycle. Proc Natl Acad Sci USA. 2001; 98:980–985. [PubMed: 11158581]

Hale CA, Meinhardt H, de Boer PAJ. Dynamic localization cycle of the cell division regulator MinE in *Escherichia coli*. EMBO J. 2001; 20:1563–1572. [PubMed: 11285221]

Hsieh C-W, Lin T-Y, Lai H-M, Lin C-C, Hsieh T-S, Shih Y-L. Direct MinE–membrane interaction contributes to the proper localization of MinDE in *E. coli*. Mol Microbiol. 2010; 75:499–512. [PubMed: 20025670]

Hu Z, Lutkenhaus J. Topological regulation of cell division in *Escherichia coli* involves rapid pole to pole oscillation of the division inhibitor MinC under the control of MinD and MinE. Mol Microbiol. 1999; 34:82–90. [PubMed: 10540287]

Hu Z, Mukherjee A, Pichoff S, Lutkenhaus J. The MinC component of the division site selection system in *Escherichia coli* interacts with FtsZ to prevent polymerization. Proc Natl Acad Sci USA. 1999; 96:14819–14824. [PubMed: 10611296]

Hu Z, Lutkenhaus J. Analysis of MinC Reveals Two Independent Domains Involved in Interaction with MinD and FtsZ. J Bacteriol. 2000; 182:3965–3971. [PubMed: 10869074]

Hu Z, Gogol EP, Lutkenhaus J. Dynamic assembly of MinD on phospholipid vesicles regulated by ATP and MinE. Proc Natl Acad Sci USA. 2002; 99:6761–6766. [PubMed: 11983867]

Hu Z, Lutkenhaus J. A conserved sequence at the C-terminus of MinD is required for binding to the membrane and targeting MinC to the septum. Mol Microbiol. 2003; 47:345–355. [PubMed: 12519187]

Ivanov V, Mizuuchi K. Proc Natl Acad Sci USA. 2010; Multiple modes of interconverting dynamic pattern formation by bacterial cell division proteins.107:8071–8078. [PubMed: 20212106]

Jamroskovic J, Pavlendova N.a. Muchova K, Wilkinson AJ, Barak I. An oscillating Min system in *Bacillus subtilis* influences asymmetrical septation during sporulation. Microbiol. 2012; 158:1972–1981.

Kawai F, Shoda M, Harashima R, Sadaie Y, Hara H, Matsumoto K. Cardiolipin Domains in *Bacillus subtilis* Marburg Membranes. J Bacteriol. 2004; 186:1475–1483. [PubMed: 14973018]

Kiekebusch D, Thanbichler M. Spatiotemporal organization of microbial cells by protein concentration gradients. Trends Microbiol. 2012; 22:65–73. [PubMed: 24342487]

Koppelman CM, Blaauwen TD, Duursma MC, Heeren RMA, Nanninga N. *Escherichia coli* Minicell Membranes Are Enriched in Cardiolipin . J Bacteriol. 2001; 183:6144–6147. [PubMed: 11567016]

Lackner LL, Raskin DM, de Boer PAJ. ATP-Dependent Interactions between *Escherichia coli* Min Proteins and the Phospholipid Membrane In Vitro. J Bacteriol. 2003; 185:735–749. [PubMed: 12533449]

Lewis RNAH, McElhaney RN. The physicochemical properties of cardiolipin bilayers and cardiolipin-containing lipid membranes. Biochim Biophys Acta. 2009; 1788:2069–2079. [PubMed: 19328771]

Loose M, Fischer-Friedrich E, Ries J, Kruse K, Schwille P. Spatial Regulators for Bacterial Cell Division Self-Organize into Surface Waves *in vitro*. Science. 2008; 320:789–792. [PubMed: 18467587]

Loose M, Fischer-Friedrich E, Herold C, Kruse K, Schwille P. Min protein patterns emerge from rapid rebinding and membrane interaction of MinE. Nat Struct Mol Biol. 2011; 18:577–583. [PubMed: 21516096]

Lopez CS, Alice AF, Heras H, Rivas EA, Sanchez-Rivas C. Role of anionic phospholipids in the adaptation of *Bacillus subtilis* to high salinity. Microbiol. 2006; 152:605–616.

Lutkenhaus J. Assembly Dynamics of the Bacterial MinCDE System and Spatial Regulation of the Z Ring. Annu Rev Biochem. 2007; 76:539–562. [PubMed: 17328675]

Mika JT, Poolman B. Macromolecule diffusion and confinement in prokaryotic cells. Curr Opin Biotechnol. 2011; 22:117–126. [PubMed: 20952181]

Mileykovskaya E, Dowhan W. Visualization of Phospholipid Domains in *Escherichia coli* by Using the Cardiolipin-Specific Fluorescent Dye 10-N-Nonyl Acridine Orange. J Bacteriol. 2000; 182:1172–1175. [PubMed: 10648548]

Mileykovskaya E, Fishov I, Fu X, Corbin BD, Margolin W, Dowhan W. Effects of Phospholipid Composition on MinD-Membrane Interactions *in vitro* and *in vivo*. J Biol Chem. 2003; 278:22193–22198. [PubMed: 12676941]

Mileykovskaya E, Ryan AC, Mo X, Lin CC, Khalaf KI, Dowhan W, Garrett TA. Phosphatidic acid and N-acylphosphatidylethanolamine form membrane domains in *Escherichia coli* mutant lacking cardiolipin and phosphatidylglycerol. J Biol Chem. 2009; 284:2990–3000. [PubMed: 19049984]

Park K-T, Wu W, Battaile KP, Lovell S, Holyoak T, Lutkenhaus J. The Min Oscillator Uses MinD-Dependent Conformational Changes in MinE to Spatially Regulate Cytokinesis. Cell. 2011; 146:396–407. [PubMed: 21816275]

Ramirez-Arcos S, Szeto J, Dillon JA, Margolin W. Conservation of dynamic localization among MinD and MinE orthologues: oscillation of Neisseria gonorrhoeae proteins in *Escherichia coli*. Mol Microbiol. 2002; 46:493–504. [PubMed: 12406224]

Raskin DM, de Boer PAJ. MinDE-Dependent Pole-to-Pole Oscillation of Division Inhibitor MinC in *Escherichia coli*. J Bacteriol. 1999; 181:6419–6424. [PubMed: 10515933]

Raskin DM, deBoer PAJ. Rapid pole-to-pole oscillation of a protein required for directing division to the middle of *Escherichia coli*. Proc Natl Acad Sci USA. 1999b; 96:4971–4976. [PubMed: 10220403]

Renner LD, Weibel DB. Cardiolipin microdomains localize to negatively curved regions of *Escherichia coli* membranes. Proc Natl Acad Sci USA. 2011; 108:6264–6269. [PubMed: 21444798]

Renner LD, Weibel DB. MinD and MinE Interact with Anionic Phospholipids and Regulate Division Plane Formation in *Escherichia coli*. J Biol Chem. 2012; 287:38835–38844. [PubMed: 23012351]

Shih YL, Huang KF, Lai HM, Liao JH, Lee CS, Chang CM, Mak HM, Hsieh CW, Lin CC. The N-terminal amphipathic helix of the topological specificity factor MinE is associated with shaping membrane curvature. PLoS One. 2011; 6:e21425. [PubMed: 21738659]

Szeto TH, Rowland SL, Rothfield LI, King GF. Membrane localization of MinD is mediated by a C-terminal motif that is conserved across eubacteria, archaea, and chloroplasts. Proc Natl Acad Sci USA. 2002; 99:15693–15698. [PubMed: 12424340]

Szeto TH, Rowland SL, Habrukowich CL, King GF. The MinD Membrane Targeting Sequence Is a Transplantable Lipid-binding Helix. J Biol Chem. 2003; 278:40050–40056. [PubMed: 12882967]

Woldringh CL, Mulder E, Huls PG, Vischer N. Toporegulation of bacterial division according to the nucleoid occlusion model. Res Microbiol. 1991; 142:309–320. [PubMed: 1925029]

Wu W, Park KT, Holyoak T, Lutkenhaus J. Determination of the structure of the MinD-ATP complex reveals the orientation of MinD on the membrane and the relative location of the binding sites for MinE and MinC. Mol Microbiol. 2011; 79:1515–1528. [PubMed: 21231967]

Vecchiarelli AG, Mizuuchi K, Funnell BE. Surfing biological surfaces: exploiting the nucleoid for partition and transport in bacteria. Mol Microbiol. 2012; 86:513–523. [PubMed: 22934804]

Vecchiarelli AG, Hwang LC, Mizuuchi K. Cell-free study of F plasmid partition provides evidence for cargo transport by a diffusion-ratchet mechanism. Proc Natl Acad Sci USA. 2013; 110:E1390–E1397. [PubMed: 23479605]

Yu X-C, Margolin W. FtsZ ring clusters in min and partition mutants: role of both the Min system and the nucleoid in regulating FtsZ ring localization. Mol Microbiol. 1999; 32:315–326. [PubMed: 10231488]

Zhou H, Lutkenhaus J. Membrane Binding by MinD Involves Insertion of Hydrophobic Residues within the C-Terminal Amphipathic Helix into the Bilayer. J Bacteriol. 2003; 185:4326–4335. [PubMed: 12867440]

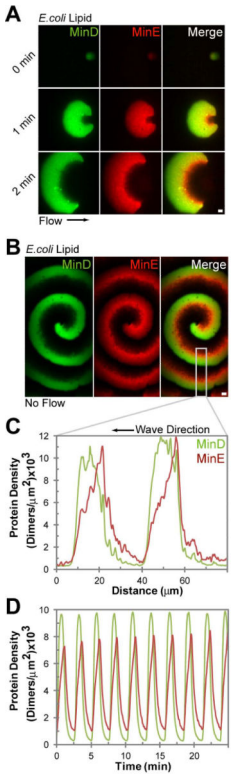

Figure 1. Flow influences Min patterning on an SLB

(A) A time-lapse image series showing a MinD/MinE initiation center breaking asymmetrically into an upstream travelling wave on an *E.coli* lipid SLB. GFP-MinD (1 μM) and 1.5 μM MinE (mixed 1:19 with MinE-Alexa 647) were preincubated with 2.5 mM ATP and infused into the flowcell at a constant flow rate of 1 μl/min from left to right. (B) Several minutes after flow stoppage, MinD and MinE formed highly regular and spiraling wave trains. For A and B, Scale bar 5 μm. (C) Cross-section of the protein densities of MinD (green) and MinE (red) within the wave train in B. (D) Time-course of MinD (green) and MinE (red) protein densities at a fixed location within the wave train in B. Time zero was chosen arbitrarily. Also see Movies S1 and S3.

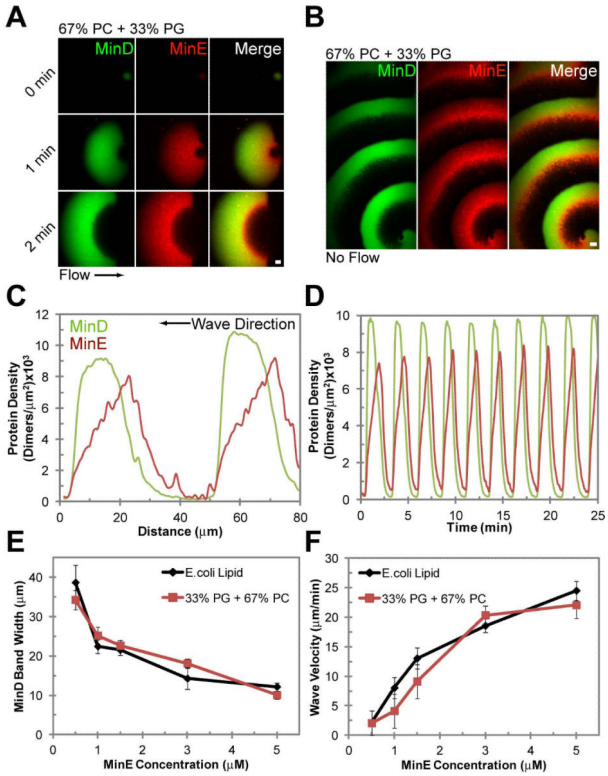

Figure 2. An SLB without cardiolipin supports Min patterns

(A) A time-lapse image series showing a MinD/MinE initiation center breaking asymmetrically into an upstream travelling wave on an mSLB. GFP-MinD (1 μM) and 1.5 μM MinE (mixed 1:19 with MinE-Alexa 647) were preincubated with 2.5 mM ATP and infused into the flowcell at a constant flow rate of 1 μl/min from left to right. (B) Several minutes after flow stoppage, MinD and MinE formed highly regular and spiraling wave trains on the mSLB. Scale bar 5 μm. (C) Cross-section of the protein densities of MinD (green) and MinE (red) within the wave train in B. (D) Time-course of MinD (green) and MinE (red) protein densities at a fixed location within the wave train in B. (E) With increasing MinE concentration in solution, MinD waves narrow to similar extents on SLBs with or without CL. MinD band widths within spiraling wave trains on an *E.coli* SLB (black line) or mSLB (red line) are plotted as a function of MinE concentration in solution. (F) With increasing MinE concentration in solution, MinD wave velocity increases to similar extents on SLBs with or without CL. MinD wave velocities on an *E.coli* SLB (black line) or mSLB (red line) are plotted as a function of MinE concentration in solution. For E and F, MinD solution concentration was held at 1 μM. Bilayer composition expressed in mol %. Error bars represent the SD for n=10 waves in at least two independent experiments. Also see Fig. S2 and Movies S4-S5.

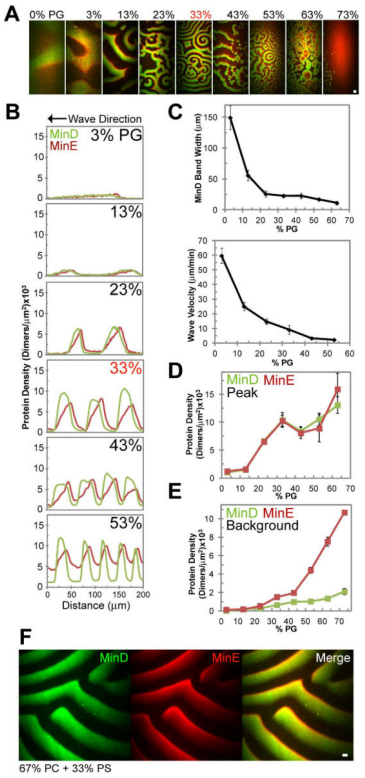

Figure 3. Anionic lipid content of SLB affects Min Patterning

(A) Freeze-frame images of the typical MinD (green) and MinE (red) patterns that form on SLBs containing the indicated PG density. The net negative charge density provided by an SLB composed of 33% PG (and 67% PC) is roughly similar to that of SLBs made with *E.coli* polar lipid extract. Images were taken at least 30 minutes after flow stoppage. Scale bar 10 μm. (B) Cross-section of the protein densities of MinD (green) and MinE (red) within wave trains that are generated at the indicated PG density of the SLB. (C) With increasing negative charge density of the SLB, MinD waves became narrower and slower in velocity. MinD band widths (top graph) and wave velocities (bottom graph) within spiraling wave trains are plotted as a function of PG density in the SLB. (D) Average protein density associated with the staggered MinD (green) and MinE (red) peaks within a wave train are plotted as a function of the PG density in the SLB. (E) MinE binds the SLB independent of MinD at high anionic lipid densities. The average MinD (green) and MinE (red) protein densities in between Min waves are plotted as a function of PG density. For C to E, error bars represent the SD for n=10 waves in at least two independent experiments. (F) Min patterns are supported with lipids not found in *E. coli*. Freeze frame image of Min patterns on a PC/PS SLB. Bilayer composition expressed in mol %. Scale bar 5 μm. Also see Movie S6.

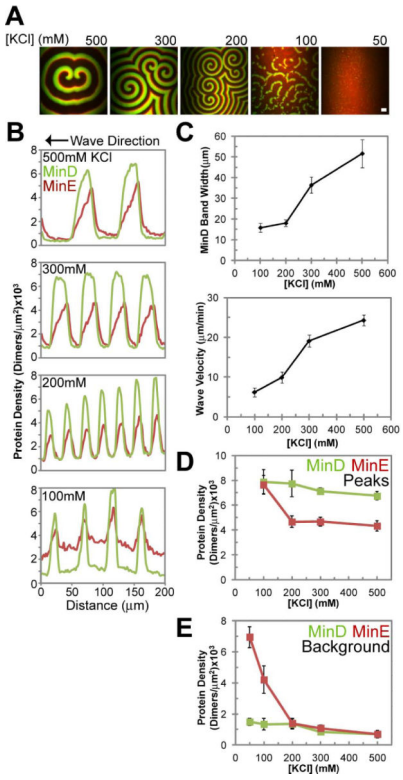

Figure 4. Salt concentration affects Min Patterning

(A) Freeze-frame images of the typical MinD (green) and MinE (red) patterns that form on an mSLB at salt concentrations indicated. Images were taken at least 30 minutes after flow stoppage. Scale bar 10 μm. (B) Cross-section of the protein densities of MinD (green) and MinE (red) within wave trains generated at the indicated salt concentration. (C) With increasing salt concentration, MinD waves became wider and faster in velocity. MinD band widths (top graph) and wave velocities (bottom graph) within spiraling wave trains are plotted as a function of salt concentration. (D) Average protein density associated with the staggered MinD (green) and MinE (red) peaks within a wave train are plotted as a function of salt concentration. (E) MinE binds SLB independent of MinD at lower ionic strengths. The average background MinD (green) and MinE (red) protein densities in between Min waves are plotted as a function of salt concentration. Bilayer composition expressed in mol %. For C to E, error bars represent the SD for n=10 waves in at least one experiment.